

Optimisation of Electrolyser Operation: Integrating External Heat

Matthias Derez

Department of Mechanical Engineering
KU Leuven
Leuven, Belgium

Alexander Hoogsteyn

Department of Mechanical Engineering
KU Leuven
Leuven, Belgium
alexander.hoogsteyn@kuleuven.be

Erik Delarue

Department of Mechanical Engineering
KU Leuven
Leuven, Belgium
erik.delarue@kuleuven.be

Abstract—Integrating external heat into electrolysers can reduce the electrical power demand for carbon-neutral hydrogen production. Efficient operation requires detailed models that incorporate heat availability and its effect on startup costs. This paper advances existing operational models by endogenously modelling startup costs and direct heat integration, based on a piecewise linear approximation of the electrochemical equations. We analyse the impact of low- and high-temperature heat integration on the efficiency and profitability of hydrogen production for solid oxide and proton exchange membrane (PEM) electrolysis technologies. Our case study demonstrates that heat integration can significantly enhance the profitability of solid oxide electrolysis, increasing average daily profits by up to 23.3%. For PEM electrolysis, the impact is more modest, with profit gains of 1.9–2.7%. Despite this, the break-even hydrogen price for solid oxide electrolysis remains high at 5.5 EUR/kg, given an investment cost of 2300 EUR/kW. PEM electrolysis achieves breakeven at more competitive hydrogen prices of 3.5–4.5 EUR/kg, depending on lifetime assumptions and an investment cost of 900 EUR/kW.

Index Terms—Hydrogen, Electrolyzer, Operation, Optimization, Renewable heat

I. INTRODUCTION

To reduce the amount of renewable electricity required for green hydrogen production, heat can be integrated into the electrolysis process. Depending on the technology heat can be added either directly to provide a share of the required enthalpy change to carry out the electrolysis reaction or indirectly in other processes in the balance of plant. Both approaches reduce the required amount of electrical energy and improve the profitability. Efficiency improvements can be achieved using a variety of low carbon energy sources: geothermal energy [1], biomass [2] or nuclear energy [3], [4], among others.

Secondly, electrolysers can increase profitability by exploiting their flexibility by adapting their hydrogen production to fluctuating electricity prices and participate in ancillary services markets [5]. However, the electrical efficiency of an electrolyser depends on the operating temperature and current density. These operating parameters can change throughout the production period, introducing variations in electrical efficiency that are often not considered [6]. Advanced operational models, capable of capturing flexibility and variable efficiency,

are necessary to accurately estimate the profits of an electrolyser [7].

To accurately represent dynamic electrolyser operation, the effect of both the temperature and current density on efficiency must be considered. This can be done by incorporating the governing electrochemical Eqs., where the chemical processes that occur and the accompanying losses are described [8]–[10]. Alternatively, empirical electrochemical models can be used that approximate the relation [11]. Such empirical models are available only for alkaline electrolysers but are nonetheless used to approximate the behaviour of proton exchange membrane (PEM) and solid oxide electrolyser (SOE) [7], [12], [13]. In this paper, operational models are developed which incorporate the original electrochemical Eqs. that relate the power consumed by the electrolyser to the operating temperature and current. To the author’s knowledge, a piecewise linearisation of the original electrochemical model Eqs. has not been carried out in the literature. [13] have approximated the empirical model by Ulleberg using a single tangent plane to the power curve at nominal power. [7] have carried out a two-dimensional piecewise linearisation of [11], where the temperature dependency is neglected, limiting the accuracy of the model to discuss the effect of heat addition.

Furthermore, the models are adapted to allow for external heat to be used in the electrolysis process. For each electrolyser type, the model is modified to make use of heat as applicable. The modelling contribution of this paper is therefore twofold; the startup behaviour is modelled more accurately, and heat addition is integrated into the models. The models are applied to a case study to discuss the results and implications of the improvements made.

II. EXTERNAL HEAT INTEGRATION

External heat integration in electrolysis technologies—such as Alkaline, Proton Exchange Membrane (PEM), and Solid Oxide Electrolysers (SOE)—can significantly enhance their performance and efficiency. SOEs, in particular, benefit greatly from external heat due to their high operating temperatures (800–1000°C), which align well with the availability of high-temperature heat sources [14]. The integration of heat in SOEs can reduce the overall electrical energy requirement by supplying part of the necessary thermal energy directly

TABLE I: Use of low- and high-temperature heat for different electrolyzers

	PEM (20-100°C) & Alkaline (40-90°C)	SOE (800-1000°C)
Low-T heat (280-325°C)	<ul style="list-style-type: none"> • Heating inlet water • Keeping temperature constant in standby • Heating electrolyser during cold start 	<ul style="list-style-type: none"> • Heating and evaporating inlet water • Heating electrolyser during cold start, in combination with an electrical heater
High-T heat (750-1000°C)		<ul style="list-style-type: none"> • Heating and evaporating inlet water • Heating steam from pinch point to operating temperature • Keeping temperature constant in standby • Heating electrolyser during cold start • Heating sweep gases to supply heat directly to the electrolyser

through external heat sources or regeneration processes. This approach allows the electrolysis process to operate below the thermoneutral voltage while keeping the operating temperature constant, reducing the electrical input needed for water electrolysis. Various auxiliary processes, such as preheating during cold start and heating during standby, are able to use external heat. An overview of the heat integration possibilities is provided in Table I.

[14] explored the effects of using external heat sources in the SOE operating range, highlighting that high-temperature heat can be employed to preheat inlet water and superheat steam using regenerative heat exchangers. This configuration obtains a system efficiency improvement of 18% by minimizing the amount of electrical energy required to achieve the high operational temperatures of the SOE. [3] evaluates the efficiency of high-temperature steam electrolytic systems coupled with various types of nuclear reactors. It specifically examines how heat from different nuclear reactor designs can be used to generate the steam needed for the electrolysis process, aiming to optimize the overall system performance.

In contrast, the Alkaline and PEM electrolyzers operate at significantly lower temperatures (20–100°C for PEM and 40–90°C for Alkaline), and cannot directly use external heat to drive the electrolysis reaction due to their inherently exothermal operating regimes. However, heat can still be beneficial for auxiliary processes, such as preheating the inlet water or maintaining the electrolyser temperature during standby modes, thereby reducing the need for electrical heating and enhancing overall system efficiency.

III. OPERATIONAL MODELS

A. Linearisation of electrochemical models

A piecewise linearisation is applied to the power curves of the PEM and SOE electrolyser. An example of such a nonconvex power curve of the SOE is shown in Figure 1 together with its division into multiple segments. Each

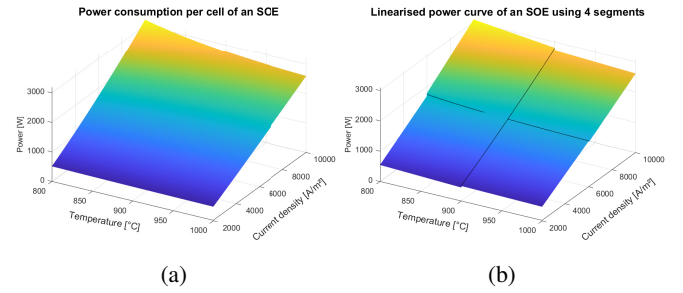


Fig. 1: (a) Power consumed per cell by a SOE as a function of temperature and current density based on the underlying electrochemical effects described in Appendix A and (b) its linearization with four segments

segment approximates the power values in its own segment by minimising the square of linearisation error. The least squares method is used to determine the coefficients a , b , and c for the best-fitting plane $P = a \cdot T + b \cdot j + c$ in each segment, where T represents temperature and j current density. For linear regression, only power values at the minimum and maximum current densities of each segment are used across the temperature range. This approach ensures linearisation is exact at the segment boundaries and avoids significant over- or underestimation at the edges, which could cause discontinuities between segments.

With one segment, the mean relative error is 4.83%, reducing to 1.14% with four segments and 0.50% with nine. Applying the same method to the PEM electrolyser, the mean relative errors for one, four, and nine segments are 13.44%, 3.32%, and 1.51%, respectively. These are higher than for the SOE due to the PEM electrolyser's larger operating current density range.

B. Solid oxide electrolyser operational model

The SOE model considers only the standby and production states, excluding the off-state due to the long cold start duration of up to 6.5 hours and the risk of thermal cycling damage associated with frequent cold starts [5]. As such, cold starts are to be avoided and omitted from the operational optimisation.¹

Drawing partly on the alkaline electrolyser model described by [13], the SOE model is formulated as follows. The objective of the operational model is to maximise profit P , as in Eq. (1), with $x = \{I_t, \dot{Q}_t^{heat}, \dot{Q}_t^{standby}, \dot{Q}_t^{cool}, p_t^b, s_t^b, S_{t,m,n}^b, \delta_t^1, T_t, p_t^{cell}\}$. Electricity prices are exogenous and vary throughout the day, while a constant hydrogen price is assumed. The decision variables include the current I [A], the heat added during production \dot{Q}_t^{heat} [W], heat added in standby $\dot{Q}_t^{standby}$ [W], cooling supplied \dot{Q}_t^{cool} [W], binary variables p_t^b and s_t^b indicating the production and standby states, the segment binary variable $S_{t,m,n}^b$ for linearisation, and the slack variable

¹Table IX shows that the number of hours in production state is high, confirming this assumption.

δ_t^1 . Temperature T_t [K] and electrolyser power p_t^{cell} [W] depend on current and temperature at prior or current timesteps.

To simplify notation, p_t^{total} , \dot{m}_t^H [kg/h], and \dot{Q}_t^{water} are introduced as expressions of the decision variables. The model Eqs. are formulated using a power curve approximation divided into M sections for temperature and N sections for current density, resulting in $M \cdot N$ segments. The Eqs. assume low-temperature heat supply to the SOE, with Δt representing the timestep duration in hours.²

$$\text{Max}_x P = \sum_{t \in \mathcal{T}} (\dot{m}_t^H \cdot \lambda^H - p_t^{total} \cdot \lambda_t^E) \cdot \Delta t \quad (1)$$

Eq.(2) describes the electrical power required without heat integration. It includes the power per cell, p_t^{cell} [W], the number of cells n_c , the total heat demand, the efficiency of the electrical heater η_{EH} , the compressor power p_t^{comp} [W], and the cooling power³. The low-temperature heat demand is used exclusively to heat water to 100°C and evaporate it, represented by $\dot{Q}_t^{water} = (c_p \Delta T_a + \Delta H) \dot{m}_t^{H_2O}$

Eq.(3) extends this formulation to include heat integration, where the heat cost is modelled as the opportunity cost of not converting the heat into electricity via a steam turbine. Most heating to operating temperature is achieved through regeneration. The final 40°C increase to reach operating temperature is applied by $\dot{Q}_t^{steam} = 40^\circ\text{C} \cdot c_p \cdot \dot{m}_t^{H_2O}$

$$p_t^{total} = n_c \cdot p_t^{cell} + \frac{\dot{Q}_t^{standby} + \dot{Q}_t^{steam} + \dot{Q}_t^{heat}}{\eta_{EH}} + \dot{Q}_t^{water} \cdot \eta_{ST} + p_t^{comp} + p_t^{cool} \quad \forall t \in \mathcal{T} \quad (2)$$

$$p_t^{total} = n_c \cdot p_t^{cell} + (\dot{Q}_t^{standby} + \dot{Q}_t^{water} + \dot{Q}_t^{steam} + \dot{Q}_t^{heat}) \cdot \eta_{ST} + p_t^{comp} + p_t^{cool} \quad \forall t \in \mathcal{T} \quad (3)$$

The hydrogen production rate is expressed using Eq. (4). The water mass flow rate in Eq. (5) follows from that. The current and temperature determine the electrical power consumption using Eq. (6). Here $a_{m,n}$, $b_{m,n}$ and $c_{m,n}$ are the coefficients of the plane that approximates the power curve in the (m, n) segment, which is located in the m^{th} current density section and the n^{th} temperature section.

$$\dot{m}_t^H = n_c M_{H_2} \frac{I_t}{2F} \quad \forall t \in \mathcal{T} \quad (4)$$

$$\dot{m}_t^{H_2O} = \frac{M_{H_2O}}{M_{H_2}} \dot{m}_t^H \quad \forall t \in \mathcal{T} \quad (5)$$

$$p_t^{cell} = \sum_{m \in M, n \in N} S_{t,m,n}^b (a_{m,n} T_t + b_{m,n} \frac{I_t}{A} + c_{m,n}) + \delta_t^1 \quad \forall t \in \mathcal{T} \quad (6)$$

The model is subject to Eq. (7)-(19). Constraints (7), (8), and (9) ensure that the binary variable representing the active segment is set to one. Eqs. (10) and (11) enforce current and

temperature limits, while Eq. (13) ensures the power is zero when not in the production state. The slack variable associated with power is constrained to zero unless in standby mode by Eq. (18). Eq.(12) governs the heating demand during standby. Compressor power is defined in Eq. (14), where α depends on the pressure ratio and compressor efficiency. Eqs. (16) and (17) set the cooling and direct heat addition variables to zero when not in the production state. Eq. (15) expresses the temperature as a function of the previous timestep, based on losses and the heat flux $\dot{Q}_t = \dot{Q}_t^{standby} + \dot{Q}_t^{heat} - \dot{Q}_t^{cool}$. Eq. (19) ensures that only one binary state variable is active at any time.

$$\sum_{m \in M, n \in N} S_{t,m,n}^b = 1 \quad \forall t \in \mathcal{T} \quad (7)$$

$$\sum_{m \in M, n \in N} S_{t,m,n}^b \underline{j}_m \leq \frac{I_t}{A} \leq \sum_{m \in M, n \in N} S_{t,m,n}^b \bar{j}_m \quad \forall t \in \mathcal{T} \quad (8)$$

$$\sum_{m \in M, n \in N} S_{t,m,n}^b \underline{T}_n \leq T_t \leq \sum_{m \in M, n \in N} S_{t,m,n}^b \bar{T}_n \quad \forall t \in \mathcal{T} \quad (9)$$

$$p_t^b \underline{j}_A \leq I_t \leq p_t^b \bar{j}_A \quad \forall t \in \mathcal{T} \quad (10)$$

$$\underline{T} \leq T_t \leq \bar{T} \quad \forall t \in \mathcal{T} \quad (11)$$

$$\frac{T_t - T_a}{R_t} s_t^b \leq \dot{Q}_t^{standby} \leq M s_t^b \quad \forall t \in \mathcal{T} \quad (12)$$

$$0 \leq p_t^{cell} \leq p_t^b \bar{p} \quad \forall t \in \mathcal{T} \quad (13)$$

$$p_t^c = \alpha \dot{m}_t^H \quad \forall t \in \mathcal{T} \quad (14)$$

$$\frac{C_h(T_t - T_{t-1})}{\Delta t} = n_c (p_{t-1}^{cell} - U_{tn} I_{t-1}) - \frac{T_{t-1} - T_a}{R_t} + \dot{Q}_{t-1} \quad \forall t \in \mathcal{T}_0 \quad (15)$$

$$0 \leq \dot{Q}_t^{cool} \leq p_t^b M \quad \forall t \in \mathcal{T} \quad (16)$$

$$0 \leq \dot{Q}_t^{heat} \leq p_t^b M \quad \forall t \in \mathcal{T} \quad (17)$$

$$-M s_t^b \leq \delta_t^1 \leq M s_t^b \quad \forall t \in \mathcal{T} \quad (18)$$

$$p_t^b + s_t^b = 1 \quad \forall t \in \mathcal{T} \quad (19)$$

C. PEM electrolyser operational model

The PEM electrolyser model includes on, off, and standby states, maximising profit P as in Eq. (20), with $x = \{I_t, \dot{Q}_t^{standby}, \dot{Q}_t^{cool}, p_t^b, s_t^b, i_t^b, Z_t^b, S_{t,m,n}^b, \delta_t^1, T_t, p_t^{cell}\}$. Cold start costs, C_t^{CS} , account for reduced hydrogen output and electricity use during start-up (Eq. (21)) and are linked to electricity and hydrogen prices for greater accuracy. Cold starts require no external heat and are assumed to last 10 minutes, while hot starts are instantaneous and cost-free, reflecting the PEM's operational flexibility.

$$\text{Max}_x P = \sum_{t \in \mathcal{T}} (\dot{m}_t^H \cdot \lambda^H - p_t^{total} \cdot \lambda_t^E) \cdot \Delta t - \sum_{t \in \mathcal{T}_0} C_t^{CS} Z_t^b \quad (20)$$

$$C_t^{CS} = \Delta t^{CS} \cdot (\dot{m}_{\underline{T}, I}^H \cdot \lambda^H - p_{\underline{T}, I}^E \cdot \lambda_t^E) \quad \forall t \in \mathcal{T} \quad (21)$$

²In this study, 15-minute intervals are modelled, setting $\Delta t = 0.25$.

³ [14] approximate the cooling power p_t^{cool} as $p_t^{cool} = \frac{\dot{Q}_t^{cool}}{400}$, where \dot{Q}_t^{cool} is the thermal cooling power

Eq. (22) calculates the total electrical power required without heat integration, while Eq. (23) includes heat integration. Heating inlet water from ambient temperature to 100°C is partially achieved through regeneration.⁴ The remaining heat demand, \dot{Q}_t^{water} , is described by Eq. (24), which assumes operation at maximum temperature and efficiency. This assumption is justified as the PEM electrolyser typically operates under these conditions, and the heat demand is minor compared to other energy requirements. Heat is used to warm inlet water and supply standby thermal power, with costs representing the opportunity cost of forgone electricity generation.

$$p_t^{total} = n_c \cdot p_t^{cell} + \frac{\dot{Q}_t^{standby} + \dot{Q}_t^{water}}{\eta_{EH}} + p_t^{comp} + p_t^{cool} \quad \forall t \in \mathcal{T} \quad (22)$$

$$p_t^{total} = n_c \cdot p_t^{cell} + (\dot{Q}_t^{standby} + \dot{Q}_t^{water}) \cdot \eta_{ST} + p_t^{comp} + p_t^{cool} \quad \forall t \in \mathcal{T} \quad (23)$$

$$\dot{Q}_t^{water} = \dot{m}_t^{H_2O} \cdot c_p^{water} \cdot \Delta T^{water} \quad \forall t \in \mathcal{T} \quad (24)$$

The model is subject to constraints (7)-(16) and (25)-(31). In Eq. (15) the heat flux is given by $\dot{Q}_t = \dot{Q}_t^{standby} - \dot{Q}_t^{CS} - \dot{Q}_t^{cool}$. With \dot{Q}_t^{CS} , as described in Eq. (25). Eqs. (26)-(31) extend the binary logic to account for the three operating states.

$$\dot{Q}_t^{CS} = \frac{\Delta t^{CS}}{\Delta t} (n_c p_{T,I} - n_c U_{tn} I) \quad \forall t \in \mathcal{T} \quad (25)$$

$$-M(s_t^b + i_t^b) \leq \delta_t^1 \leq M(s_t^b + i_t^b) \quad \forall t \in \mathcal{T} \quad (26)$$

$$p_t^b + s_t^b + i_t^b = 1 \quad \forall t \in \mathcal{T} \quad (27)$$

$$s_t^b + i_{t-1}^b \leq 1 \quad \forall t \in \mathcal{T}_0 \quad (28)$$

$$s_{t-1}^b + i_t^b \leq 1 \quad \forall t \in \mathcal{T}_0 \quad (29)$$

$$i_{t-1}^b + p_t^b - 1 \leq Z_t^b \leq i_{t-1}^b \quad \forall t \in \mathcal{T}_0 \quad (30)$$

$$Z_t^b \leq p_t^b \quad \forall t \in \mathcal{T}_0 \quad (31)$$

IV. CASE STUDY

A. Data & cases

This section applies the models from Section III to a case study. The linearised models were implemented in Julia and solved using Gurobi.⁵ Electrolyser parameters are scaled to consume 15 MW of electrical power at maximum temperature and current density (see C). To assess profitability and the impact of heat integration, daily profits are calculated for each day of a full year using 2019 Belgian day-ahead electricity prices, avoiding distortions from COVID-19 and the energy crisis. Hydrogen price levels range from 2.5 to 5.5 EUR/kg.

A rolling horizon approach optimises daily operation independently. The final operational state and temperature from each day serve as starting conditions for the next, ensuring realistic transitions and startup costs.⁶

⁴We determined that the outlet hydrogen stream at 100°C can heat inlet water from 20°C to 46.8°C, leaving $\Delta T^{water} = 53.2^\circ\text{C}$; details in [15]

⁵The Julia implementation is publicly available at: <https://github.com/Matthias-Derez/Electrolyser-Models>

⁶Validation was performed by comparing rolling horizon results to full-week optimisations for randomly selected weeks.

We consider five cases: 1) The case *SOE without heat integration* serves as a reference for the SOE model in which no heat integration is applied in any form. Hence, Eq. (2) applies, and \dot{Q}_t^{heat} is constraint to zero. 2) In the case *SOE with low-T heat integration* external heat is used in standby and during start-up. So, Eq. (3) applies, but \dot{Q}_t^{heat} is constraint to zero. 3) In the case *SOE with high-T integration*, direct addition of external heat is considered, which reduces the electrical power required. Hence, Eq. (3) applies, and \dot{Q}_t^{heat} is nonzero. 4) The case *PEM without heat integration* serves as a reference for the PEM model in which no heat integration is applied in any form. Hence, Eq. (22) applies. 5) In the case *PEM with heat integration*, external heat is used in standby and during start-up. Therefore, Eq. (23) applies.

B. Results heat integration in a SOE

Figures 2a and 2b illustrate the typical operation of the SOE model without heat integration over one day. Figure 2a depicts day-ahead electricity prices and electrolyser power, while Figure 2b shows temperature evolution, with bar colours indicating operational states. During periods of high electricity prices, the electrolyser enters standby. At the thermoneutral voltage temperature of 900°C (achieved at a current density of 10,000 A/m²), no external heating is needed. Operating above this temperature increases efficiency but reduces profit due to higher heating costs, while operating below it reduces efficiency and is avoided unless standby is anticipated.

Integrating heat significantly improves profitability. Low-temperature heat increases profits by 17.1% – 4.0% for hydrogen prices of 2.5–5.5 EUR/kg, while high-temperature heat further increases profits by 23.3% – 5.4%. Table II summarises these relative improvements.

The system efficiency increases from 77.77% without heat integration to 85.63% with low-temperature heat and 88.73% with high-temperature heat. These values align with the literature: efficiencies of 76 – 81% (LHV basis) without heat integration [16] and 89.5% with high-temperature heat [10]. Efficiency remains constant across hydrogen prices, as even at 2.5 EUR/kg, marginal production costs are covered for most hours.

Profitability was assessed by comparing profits with investment costs. Based on [5], a 15 MW SOE costs 34.5 MEUR. Assuming a 20,000-hour lifetime and a 3% discount rate, break-even analysis reveals that average daily profits are generally insufficient to cover investment costs, due to high capital costs and limited lifetime. Only at 5.5 EUR/kg hydrogen, with low-cost heat integration, is profitability sufficient to break even. Detailed results are presented in Table IX in Appendix C.

C. Results heat integration in a PEM

Figures 3a and 3b show an example of typical PEM electrolyser behaviour, using the *PEM without heat integration* model. Because water electrolysis is an exotherm process, the temperature is close to the maximum temperature during operation. Furthermore, the off-state is preferred over the

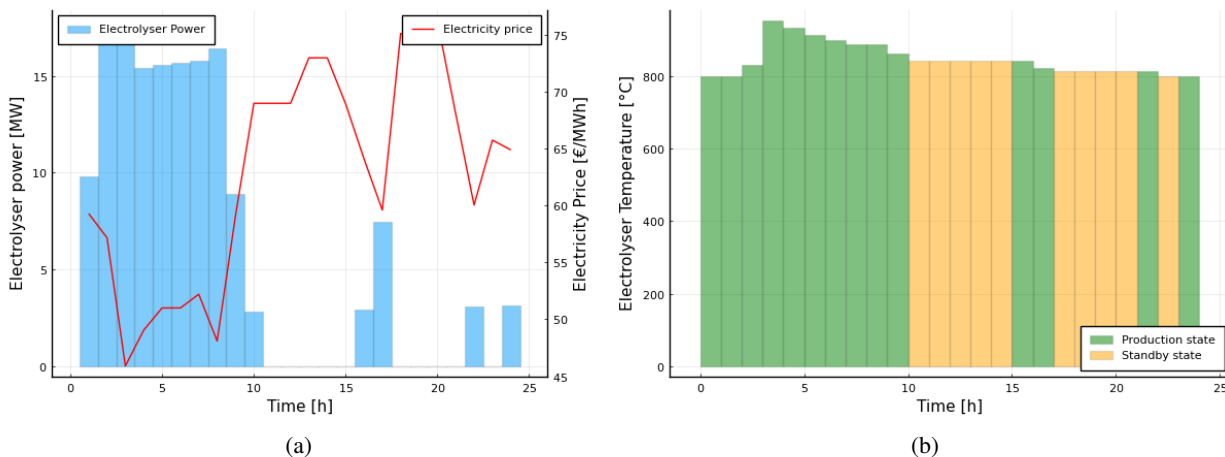


Fig. 2: (a) SOE power and electricity price, and (b) temperature and operational state, for 5th Jan 2019 using 2.5 EUR/kg H₂

Hydrogen Price (EUR/kg)	SOE with low-T heat (%)	SOE with high-T heat (%)	PEM with low/high-T heat (%)
2.5	17	23	1.8
3.5	8	12	1
4.5	6	8	0.6
5.5	4	6	0.4

TABLE II: Relative improvement in average profit per day for a SOE and PEM for different degrees of heat integration, compared to no heat integration

standby state, as the temperature can increase rapidly after a cold start. The impact of an external low-cost heat source on profitability is modest, increasing average daily profits by just 1.83% – 0.44%, as shown in Table II. This is because the off-state is generally preferred over standby, and the heat required to bring water to operating temperature is minimal compared to other energy demands.

For PEM electrolyzers, power loading significantly influences efficiency, making partial loading a viable strategy when operating near marginal costs. This trade-off arises from the wide current density range, which leads to substantial efficiency variations. For instance, at 1500 A/m², the hydrogen production rate is low but efficient, resulting in low marginal costs. Conversely, at 20,000 A/m², production is high but less efficient, with higher marginal costs. This efficiency-cost balance can lead to suboptimal results and relatively low daily profits depending on electricity and hydrogen prices.

Compared to SOE, the lower capital costs and longer lifetimes of PEM electrolyzers make them more economically viable in certain scenarios. Assuming an 80,000-hour lifetime, average daily profits are sufficient to cover investment costs at a hydrogen price of 3.5 EUR/kg. For a 50,000-hour lifetime, this threshold rises to 4.5 EUR/kg. These calculations use a CAPEX of 900 EUR/kW, based on [5].⁷

⁷The numerical results are contingent on the specific year of electricity price data and the nominal power of the electrolyser.

V. CONCLUSION

This study develops operational models for SOE and PEM electrolyzers, incorporating electrochemical equations that relate power consumption to temperature and current density. The models are enhanced to integrate external heat sources, using a piecewise-linear approximation of the power curve. Startup costs are refined to better reflect real electrolyser behaviour in response to instantaneous electricity prices.

We examine key characteristics of these technologies, focusing on the impact of temperature and direct heat supply on efficiency. Increasing temperature reduces irreversible losses, improving efficiency, while direct heat integration allows SOE to reduce electrical power consumption, boosting overall efficiency. PEM electrolyzers cannot directly use external heat for operation but can benefit from heat to maintain standby mode, a feature both technologies can utilise.

A case study of a 15 MW PEM and SOE estimates profit increases from heat integration. The SOE’s daily profits rise by up to 23.3%, while PEM profits increase by just 1.83%. However, despite heat integration, the SOE requires a hydrogen price of 5.5 EUR/kg to break even, and PEM electrolyser costs remain lower due to a more favourable CAPEX and longer lifetime. Heat integration does not significantly reduce the break-even price for PEM.

The models developed in this paper can be used to plan the optimal dispatch of the different electrolyser types. However, because of their efficient formulation, the models can also be used in energy system models, e.g., for planning studies, where a constant electrolyser efficiency is often assumed. The models developed in this study take into account the varying electrolyser efficiency and increase the accuracy of the results.

REFERENCES

- [1] J. Sigurvinsson, C. Mansilla, P. Lovera, and F. Werkoff, “Can high temperature steam electrolysis function with geothermal heat?” *International Journal of Hydrogen Energy*, vol. 32, pp. 1174–1182, 06 2007.

- [2] C. B. R. Rivera-Tinoco, C. Mansilla and F. Werkoff, "On the possibilities of producing hydrogen by high temperature electrolysis of water steam supplied from biomass or waste incineration units," *International Journal of Green Energy*, vol. 5, no. 5, pp. 388–404, 2008. [Online]. Available: <https://doi.org/10.1080/15435070802414322>
- [3] W. Zhang, B. Yu, and J. Xu, "Efficiency evaluation of high-temperature steam electrolytic systems coupled with different nuclear reactors," *International Journal of Hydrogen Energy*, vol. 37, no. 17, pp. 12060–12068, Sep. 2012. [Online]. Available: <https://www.sciencedirect.com/science/article/pii/S0360319912008786>
- [4] J. E. O'Brien, M. G. McKellar, and E. A. Harvego, "High-temperature electrolysis for large-scale hydrogen and syngas production from nuclear energy – summary of system simulation and economic analyses," *International Journal of Hydrogen Energy*, vol. 35, no. 10, pp. 4808–4819, May 2010.
- [5] IRENA, "Green hydrogen cost reduction: Scaling up electrolyzers to meet the 1.5C climate goal," IRENA International Renewable Energy Agency, Tech. Rep., Dec. 2020, <https://www.irena.org/publications/2020/Dec/Green-hydrogen-cost-reduction>. Last accessed 04/06/2023.
- [6] J. Park, S. Kang, S. Kim, H.-S. Cho, S. Heo, and J. H. Lee, "Techno-economic analysis of solar powered green hydrogen system based on multi-objective optimization of economics and productivity," *Energy Conversion and Management*, vol. 299, p. 117823, Jan. 2024. [Online]. Available: <https://www.sciencedirect.com/science/article/pii/S019689042301169X>
- [7] M. T. Baumhof, E. Raheli, A. G. Johnsen, and J. Kazempour, "Optimization of Hybrid Power Plants: When Is a Detailed Electrolyzer Model Necessary?" Jan. 2023. [Online]. Available: <http://arxiv.org/abs/2301.05310>
- [8] Z. Abidin, C. J. Webb, and E. M. Gray, "Modelling and simulation of a proton exchange membrane (PEM) electrolyser cell," *International Journal of Hydrogen Energy*, vol. 40, no. 39, pp. 13243–13257, Oct. 2015. [Online]. Available: <https://www.sciencedirect.com/science/article/pii/S0360319915019321>
- [9] I. Firtina-Ertis, "Thermodynamic and electrochemical assessment of an alkaline electrolyzer (AE) at different operating parameters," *Journal of Environmental Chemical Engineering*, vol. 10, no. 2, Apr. 2022. [Online]. Available: <https://www.sciencedirect.com/science/article/pii/S2213343722000987>
- [10] Y. Zhao, H. Xue, X. Jin, B. Xion, R. Liu, Y. Peng, L. Jiang, and G. Tian, "System level heat integration and efficiency analysis of hydrogen production process based on solid oxide electrolysis cells," *International Journal of Hydrogen Energy*, vol. 46, no. 77, pp. 38163–38174, Nov. 2021. [Online]. Available: <https://www.sciencedirect.com/science/article/pii/S0360319921036077>
- [11] O. Ulleberg, "Modeling of advanced alkaline electrolyzers: a system simulation approach," *International Journal of Hydrogen Energy*, vol. 28, no. 1, pp. 21–33, Jan. 2003. [Online]. Available: <https://www.sciencedirect.com/science/article/pii/S0360319902000332>
- [12] C. Varela, M. Mostafa, and E. Zondervan, "Modeling alkaline water electrolysis for power-to-x applications: A scheduling approach," *International Journal of Hydrogen Energy*, vol. 46, no. 14, pp. 9303–9313, Feb. 2021. [Online]. Available: <https://www.sciencedirect.com/science/article/pii/S036031992034725X>
- [13] Y. Zheng, S. You, H. W. Bindner, and M. Munster, "Optimal day-ahead dispatch of an alkaline electrolyser system concerning thermal–electric properties and state-transitional dynamics," *Applied Energy*, vol. 307, Feb. 2022. [Online]. Available: <https://www.sciencedirect.com/science/article/pii/S0306261921013751>
- [14] F. Petipas, A. Brisse, and C. Bouallou, "Benefits of external heat sources for high temperature electrolyser systems," *International Journal of Hydrogen Energy*, vol. 39, no. 11, pp. 5505–5513, Apr. 2014. [Online]. Available: <https://www.sciencedirect.com/science/article/pii/S0360319914002596>
- [15] M. Derez, "Improvement of electrochemical representation and integration of heat in electrolyser operational models," Master Thesis, Jun. 2023.
- [16] A. Kecebas, M. Kayfeci, and M. Bayat, "Electrochemical hydrogen generation," in *Solar Hydrogen Production*. Academic Press, Jan. 2019, pp. 299–317. [Online]. Available: <https://www.sciencedirect.com/science/article/pii/B9780128148532000096>
- [17] A. Buttler, R. Koltun, R. Wolf, and H. Spliethoff, "A detailed techno-economic analysis of heat integration in high temperature electrolysis for efficient hydrogen production," *International Journal of Hydrogen Energy*, vol. 40, no. 1, pp. 38–50, Jan. 2015. [Online]. Available: <https://www.sciencedirect.com/science/article/pii/S0360319914028511>
- [18] R. Yin, L. Sun, A. Khosravi, M. Malekan, and X. Shi, "Control-oriented dynamic modeling and thermodynamic analysis of solid oxide electrolysis system," *Energy Conversion and Management*, vol. 271, Nov. 2022. [Online]. Available: <https://www.sciencedirect.com/science/article/pii/S0196890422011098>
- [19] A. Chitsaz, M. A. Haghghi, and J. Hosseinpour, "Thermodynamic and exergoeconomic analyses of a proton exchange membrane fuel cell (PEMFC) system and the feasibility evaluation of integrating with a proton exchange membrane electrolyzer (PEME)," *Energy Conversion and Management*, vol. 186, pp. 487–499, Apr. 2019. [Online]. Available: <https://www.sciencedirect.com/science/article/pii/S0196890419302717>
- [20] M. Carmo, D. L. Fritz, J. Mergel, and D. Stolten, "A comprehensive review on PEM water electrolysis," *International Journal of Hydrogen Energy*, vol. 38, no. 12, pp. 4901–4934, Apr. 2013. [Online]. Available: <https://www.sciencedirect.com/science/article/pii/S0360319913002607>
- [21] A. Hernandez-Gomez, V. Ramirez, and D. Guilbert, "Investigation of PEM electrolyzer modeling: Electrical domain, efficiency, and specific energy consumption," *International Journal of Hydrogen Energy*, vol. 45, no. 29, pp. 14625–14639, May 2020. [Online]. Available: <https://www.sciencedirect.com/science/article/pii/S0360319920312271>

APPENDIX

This appendix discusses the different electrochemical electrolyser models, describing the relation between the electrical power consumption, the operating temperature and the current density of the considered electrolyser types. Using Eq. (32), the electrical power can be written as a function of temperature and current density.

$$P_{cell} = U \cdot I \quad (32)$$

Electrolysis is no reversible process but has associated losses. The cell voltage can be represented by a reversible potential U_{rev} and three overpotentials, as in Eq. (33): i) the activation overpotential U_{act} represents the voltage required to overcome the activation energy of the chemical reaction; ii) the ohmic overpotential U_{ohm} the voltage to overcome the finite electrical conductivity of the electrodes and electrolyte; and iii) the concentration overpotential U_{conc} needed due to limited mass transfer at the porous electrodes, which limit reaction kinetics [17].⁸

$$U = U_{rev} + U_{act} + U_{ohm} + U_{conc} \quad (33)$$

A. Solid oxide electrolyser electrochemical model

Using the Nernst equation, the reversible voltage can be written as a function of temperature and partial pressures, given in Eq. (34) [10]. Here T is the temperature [K], p_{H_2} , p_{O_2} and p_{H_2O} are the partial pressures [bar] of H_2 , O_2 and H_2O respectively and R is the universal gas constant [J/(mol K)]. The activation overpotential is given by [17] (35). With the Faraday constant F [C/mol], the current density j [A/m²]. The ohmic overpotential can be written as a function of the thickness d_c , d_e and d_a [m] and conductivity σ_c , σ_e and σ_a [$\Omega^{-1}m^{-1}$] of the cathode, electrolyte and anode respectively [17], [18].⁹ The concentration overpotential depends on the

⁸This equation is valid for all three electrolyser types. However, the magnitudes of the overpotentials differ between technologies

⁹The conductivity of the electrodes is assumed to be constant, while the electrolyte conductivity depends on the temperature and is given by $\sigma_{electrolyte}(T) = 33.4 \cdot 10^3 \exp\left(\frac{-10.3 \cdot 10^3}{T}\right)$ [18].

rate at which reactants approach and products leave the electrodes, resulting in the dependency on the partial pressures of the reagents and reaction products shown in Eq. (37) [10]. $D_{H_2O}^{eff}$ [m²/s] represents the effective diffusion coefficient, μ [10⁻⁷Pa·s] the dynamic viscosity of oxygen and B_g [m²] the permeability.¹⁰

$$U_{rev}^{SOE} = 1.253 - 2.4516 \cdot 10^{-4} \cdot T + \frac{RT}{2F} \ln \left(\frac{p_{H_2} \cdot (p_{O_2})^{1/2}}{p_{H_2O}} \right) \quad (34)$$

$$U_{act}^{SOE} = \frac{RT}{F} \sinh^{-1} \left(\frac{j}{2\gamma_i \cdot \exp(-\frac{E_{act,a}}{RT})} \right) + \frac{RT}{F} \sinh^{-1} \left(\frac{j}{2\gamma_i \cdot \exp(-\frac{E_{act,c}}{RT})} \right) \quad (35)$$

$$U_{ohm}^{SOE} = j \left(\frac{d_c}{\sigma_c} + \frac{d_e}{\sigma_e(T)} + \frac{d_a}{\sigma_a} \right) \quad (36)$$

$$U_{conc}^{SOE} = \frac{RT}{2F} \ln \left(\frac{1 + \frac{jRTd_c}{2Fp_{H_2}D_{H_2O}^{eff}}}{1 - \frac{jRTd_c}{2Fp_{H_2}D_{H_2O}^{eff}}} \right) + \frac{RT}{4F} \ln \left(\frac{\sqrt{(p_{O_2}^2 + \frac{jRT\mu d_a}{2FB_g})}}{p_{O_2}} \right) \quad (37)$$

B. PEM electrolyser electrochemical model

The Nernst equation can be used to represent the reversible overpotential of the PEM electrolyser as well, albeit again in a slightly adapted form shown in Eq. (38) [8]. For the PEM electrolyser, there is no aqueous *KOH* solution since the electrolyte is a solid. Because of the pure water, the water activity a_w is equal to one [8]. The activation overpotential can be represented by Eq. (39) [19]. As was the case for the AWE, α represents the electrons' transfer coefficient. For the PEM electrolyser, it is reasonable to assume that α is equal to 0.5 for both the cathode and anode [8]. [20] discuss the wide range of values for the exchange current densities of a PEM electrolyser appearing in the literature. For the anode exchange current density, values between 10⁻¹² A/m² and 1.3 · 10⁻³ A/m² are reported, while the values for the cathode exchange current density can range from 10⁻³ A/m² to 1.8 · 10⁻¹ A/m². On average, the cathode exchange current density is a factor 10⁴ larger than the anode exchange current density. The influence of the catalyst, temperature, electrode material and porosity again constitute the wide range of values present in the literature. To be able to include the effect of temperature on the exchange current densities, the following equations are used, with $j_{0,ref}$ equal to 1.08 · 10⁻¹⁷ A/m² [19]. The ohmic overpotential depends on the thickness d and conductivity σ of the different elements [8].¹¹ The concentration overpotential is

¹⁰Details on how these coefficients can be determined are given in [10]

¹¹The conductivity of the electrode $\sigma_{electrode}$ in $\Omega^{-1}m^{-1}$ is assumed to be constant, whereas the membrane conductivity $\sigma_{membrane}$ depends on the temperature: $\sigma_{membrane}(T) = (0.0439T - 3.8084) \cdot \exp(1268(\frac{1}{303} - \frac{1}{T}))$ [8], [21].

given by Equation (41) [9], where j_L is the limiting current density.¹²

$$U_{rev}^{PEM} = 1.229 - 0.9 \cdot 10^{-3} \cdot (T - 298) + \frac{RT}{2F} \cdot \ln \left(\frac{p_{H_2} \cdot p_{O_2}^{1/2}}{a_w} \right) \quad (38)$$

$$U_{act}^{PEM} = \frac{RT}{\alpha 2F} \ln \left(\frac{j}{j_{0,ref} \cdot 10^4 \cdot \exp(0.086T)} \right) + \frac{RT}{\alpha 2F} \ln \left(\frac{j}{j_{0,ref} \cdot \exp(0.086T)} \right) \quad (39)$$

$$U_{ohm}^{PEM} = \left(\frac{d_{electrode}}{\sigma_{electrode}} + \frac{d_{membrane}}{\sigma_{membrane}(T)} \right) \quad (40)$$

$$U_{conc}^{PEM} = -\frac{2RT}{F} \cdot \ln \left(1 - \frac{j}{j_L} \right) \quad (41)$$

C. Parameters

Symbol	Value	Symbol	Value
$E_{act,c}$	10 ⁵ J/mol	$E_{act,a}$	1.2 · 10 ⁵ J/mol
p_{H_2}	0.5 bar	d_{cath}	50 · 10 ⁻⁵ m
p_{O_2}	1 bar	d_{anode}	50 · 10 ⁻⁶ m
p_{H_2O}	0.5 bar	d_{elec}	50 · 10 ⁻⁶ m
γ_c	1.3 · 10 ¹⁰ A/m ²	σ_{cath}	8.4 · 10 ³ /($\Omega \cdot m$)
γ_a	2.1 A/m ²	σ_{anode}	8 · 10 ⁴ /($\Omega \cdot m$)

TABLE III: Parameters used in the SOE electrochemical model [10], [17], [18]

Symbol	Value	Symbol	Value
α	0.5	$j_{0,ref}$	1.08 · 10 ⁻¹⁷ A/m ²
p_{H_2}	1 bar	$d_{membrane}$	2.54 · 10 ⁻⁴ m
p_{O_2}	1 bar	$d_{electrode}$	8 · 10 ⁻⁴ m
a_w	1 bar	$\sigma_{electrode}$	5.53 · 10 ⁶ ($\Omega \cdot m$) ⁻¹

TABLE IV: Parameters used in the PEM electrolyser electrochemical model [8], [10], [19]

Symbol	Value	Symbol	Value
Δt	1h	M	10 ⁷
η_{EH}	0.95 [14]	c_p^{water}	4184 J/(kg·K)
η_{ST}	0.45 [17]	c_p^{steam}	2323 J/(kg·K)
M_{H_2}	2.016 · 10 ⁻³ kg/mol	ΔH	2.256 · 10 ⁶ J/kg
M_{H_2O}	18.016 · 10 ⁻³ kg/mol	T_a	293 K
\bar{p}	20 · 10 ⁶ W	α	2.92 · 10 ⁶ W·s/kg
A	0.21 m ²		

TABLE V: General parameters used in all operational models

Symbol	Value	Symbol	Value
n_c	5776	\bar{T}	1273 K
C_h	$173.28 \cdot 10^6$ J/K	T	1073 K
R_t	$1.3067 \cdot 10^{-3}$ K/W	\bar{j}	10000 A/m ²
U_{tn}	1.2995 V	\underline{j}	2000 A/m ²

TABLE VI: Parameters used in SOE operational model

Symbol	Value	Symbol	Value
n_c	1532	\bar{T}	373 K
$\dot{m}_{T,I}^H$	$29.1 \cdot 10^{-3}$ kg/s	T	293 K
$p_{T,I}^E$	$5.9 \cdot 10^6$ W	\bar{j}	20000 A/m ²
C_h	$45.96 \cdot 10^6$ J/K	\underline{j}	1500 A/m ²
R_t	$1.067 \cdot 10^{-4}$ K/W	U_{tn}	1.4813 V

TABLE VII: Parameters used in PEM operational model

D. Extra results case study

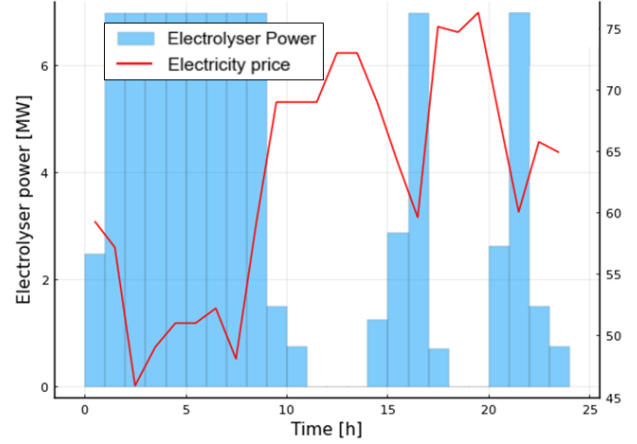
		Average profit/day [EUR]	Hours/y in production state [h]	Required profit/day [EUR]
2.5 EUR/kg H ₂	Model 1)	9053	8473	41479
	Model 2)	10597	8616	42155
	Model 3)	11158	8600	42079
3.5 EUR/kg H ₂	Model 1)	19763	8742	42750
	Model 2)	21431	8754	42807
	Model 3)	21999	8753	42802
4.5 EUR/kg H ₂	Model 1)	30694	8760	
	Model 2)	32374	8760	
	Model 3)	32943	8760	
5.5 EUR/kg H ₂	Model 1)	41642	8760	
	Model 2)	4332	8760	
	Model 3)	43891	8760	

TABLE IX: Results for a 15 MW SOE for different hydrogen prices, where the following notation is used: Model 1) SOE without heat integration, Model 2) SOE with low-temperature heat integration, Model 3) SOE with high-temperature heat integration

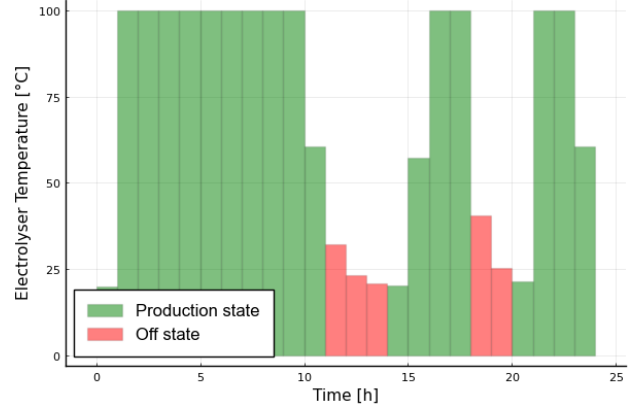
¹²To prevent the overpotential from going to infinity at the maximum current density, the limiting current density is often set to $1.05 \cdot j_{max}$ [9].

Symbol	SOE	PEM	Unit
$a_{1,1}$	-0.926	-8.253	W/K
$a_{2,1}$	-2.873	-28.833	W/K
$a_{1,2}$	-0.385	-6.942	W/K
$a_{2,2}$	-1.199	-20.188	W/K
$b_{1,1}$	0.285	0.517	W/(A/m ²)
$b_{2,1}$	0.327	0.675	W/(A/m ²)
$b_{1,2}$	0.262	0.464	W/(A/m ²)
$b_{2,2}$	0.284	0.588	W/(A/m ²)
$c_{1,1}$	968.642	2453.652	W
$c_{2,1}$	2906.471	7185.014	W
$c_{1,2}$	431.063	2352.914	W
$c_{2,2}$	1290.996	5684.778	W

TABLE VIII: Coefficients of the piecewise linearisation of the power curve of each electrolyser type using four segments



(a)



(b)

Fig. 3: (a) PEM power and electricity price and (b) temperature and operational states, for 5th Jan 2019 using 3.5 EUR/kg H₂

		Average profit/day [EUR]	Hours/y in production state [h]	Required profit/day [EUR]
2.5 EUR/kg H ₂	Model 4)	2040	7255	3677-5544
	Model 5)	2077	7114	3616-5447
3.5 EUR/kg H ₂	Model 4)	6227	8578	4243-6455
	Model 5)	6288	8547	4230-6434
4.5 EUR/kg H ₂	Model 4)	11594	8740	4313-6567
	Model 5)	11667	8737	4311-6564
5.5 EUR/kg H ₂	Model 4)	17298	8759	4321-6580
	Model 5)	17373	8758	4230-6579

TABLE X: Results for a 15 MW PEM electrolyser for different hydrogen prices, where the following notation is used: Model 4) PEM without heat integration, Model 5) PEM with heat integration